JOURNAL OF MAGNETIC RESONANCE 98, 576–588 (1992)

The Concentric Loop–Gap Resonator—A Compact, Broadly Tunable Design for NMR Applications*

MICHAEL F. KOSKINEN AND KENNETH R. METZ†

Magnetic Resonance Research Laboratory, Department of Radiology, New England Deaconess Hospital and Harvard Medical School, 185 Pilgrim Road, Boston, Massachusetts 02215

Received October 16, 1991

A loop–gap resonator design is described for use in NMR applications. Previously reported versions have employed discrete capacitors at the "gap," which typically yields a very limited tuning range. The resonator described here uses one or more concentric tuning cylinders around the inner loop to permit tuning over a range of several hundred megahertz. Construction is straightforward, the Q is high, and the excellent inherent RF field homogeneity of the loop–gap resonator is retained. A simple theoretical model for the operation of this device is presented and verified experimentally. The performance of this concentric loop–gap resonator has proven excellent for ^1H and ^{19}F NMR imaging and spectroscopy at 4.7 T. © 1992 Academic Press, Inc.

One of the primary factors affecting data quality in magnetic resonance is the RF coil design. The ideal coil would possess several properties. For optimum sensitivity and short RF pulse widths, it should have a high Q and a good filling factor. Also, in most NMR applications, a homogeneous RF field is desirable. A high self-resonance frequency is an asset, since this determines the upper limit of the RF tuning range. Several other characteristics can significantly enhance the versatility of the design, including a wide tuning range, capability for double tuning, ease of construction, and a convenient geometry for the particular magnet and sample orientation.

Among the multitude of coil designs in common use, no single type incorporates all of the desirable characteristics. The solenoid possesses a good filling factor, high Q, homogeneous B_1 field, and wide tunability (*1, 2*). However, its geometry is not well suited for use in superconducting magnets. Also, the self-resonance frequency is relatively low unless the turns are connected in parallel instead of in series (*3*). The saddle coil (*2, 4, 5*) has a better geometry for use in modern solenoidal magnets, since its B_1 field is orthogonal to the longitudinal axis of the coil. The field is relatively homogeneous although the coil can be modified to produce a gradient (*4, 6*). Unfortunately, self-resonance typically occurs at a low frequency. The birdcage coil, like

* Presented in preliminary form at the 31st Experimental NMR Conference, Pacific Grove, California, April 1–5, 1990.

† To whom correspondence should be addressed.

0022-2364/92 $5.00

the saddle coil, is based on an LC delay line concept (*7–12*). This design produces a transverse RF field with excellent homogeneity and can be double-tuned (*13–16*). The primary disadvantage of the birdcage coil is its structural complexity and difficulty in construction. The surface coil (*17*) is simple to build, has a good filling factor, a reasonably high Q, a wide tuning range, and an extremely versatile geometry (*18*). On the other hand, the B_1 field is very inhomogeneous (*19, 20*), a potentially serious disadvantage unless an RF gradient is desired for spatial localization (*21–26*) or imaging (*27–32*) experiments.

Several useful RF coil designs have evolved from the concept of a tuned cavity. For example, the coaxial cavity resonator (*33, 34*) has a good filling factor and high self-resonance frequency and is easy to construct. However, tunability is limited and the Q can be low. The slotted tube resonator (*1, 35*), which is based on a quarter-wave transmission line, also resonates at high frequencies and has the additional advantage of reasonable B_1 homogeneity. The filling factor suffers when the resonator is tuned over a wide range of frequencies. Another design based on a $\lambda/4$ transmission line has recently been reported (*36*). Alderman and Grant (*37*) described a slotted tube resonator with a homogeneous RF field, wide tunability, and high Q. This version has been employed extensively for imaging, as well as in spectroscopic applications (*38–42*). Another design was introduced by Hardy and Whitehead as the split-ring resonator (*43*) and is now usually called a loop–gap resonator (LGR). The advantages of this design include excellent RF homogeneity, an extremely high Q, a self-resonance frequency well above the present NMR range, and a filling factor equivalent to that of a solenoid (*44–50*). Like the solenoid, the B_1 field orientation is axial, a potential inconvenience when using superconducting magnets. We present here a simple modification to the standard LGR design which provides a large tuning range and simplicity of construction. The properties of this coil make it suitable for many applications in NMR spectroscopy and imaging.

PREVIOUS LGR DESIGNS

The simplest form of the LGR useful for NMR is represented in Fig. 1A. The resonator is driven inductively with an untuned coupling loop connected in the usual manner to the spectrometer transcoupler. The LGR can be viewed approximately as a series-tuned resonance circuit which depends on the inductance L of the conductive cylinder (the "loop") and the capacitance C of the "gap." Therefore, the normal equation for the resonance frequency ν applies:

$$\nu = \frac{1}{2\pi\sqrt{LC}}. \qquad [1]$$

If a simple cylindrical loop is used, it may be modeled as a single-turn solenoid of finite length. The inductance is then determined by the radius r and length l of the cylinder (*51*):

$$L = \frac{\mu\pi r^2}{l + 0.9r}, \qquad [2]$$

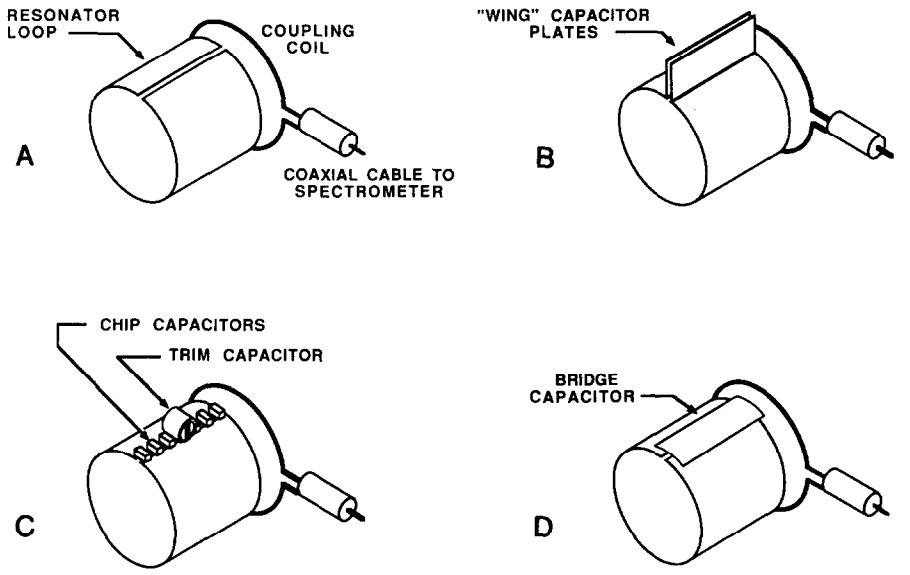

FIG. 1. Loop–gap resonator designs. (A) Simplified LGR showing the resonant loop and gap. (B) LGR with "wing" capacitor formed by extending the conductive surface at the gap. (C) LGR with gap capacitance formed by discrete chip and trimmer capacitors. (D) Bridged LGR design with small conductive plate centered above the gap.

where $\mu = 1.257 \times 10^{-8}$ H/cm for free space (*52*). Once the loop dimensions have been fixed, the tuning of the resonator can be varied by changing the capacitance at the gap.

As would be expected, most LGR designs differ mainly in the nature of the gap capacitor. The most widely employed version (*43, 44, 46*) simply extends the loop surface at the gap, forming a "wing" capacitor of two parallel plates (Fig. 1B). Insertion of a dielectric material between the plates and a "squeezing" mechanism allows the capacitance to be trimmed slightly by varying the distance between the plates. The tuning range of this design is limited by the compressibility of the dielectric. In addition, the large capacitance needed for tuning at NMR frequencies can require a wing which is large and clumsy. A more compact design (*47*) uses densely packed discrete chip capacitors distributed along the gap (Fig. 1C). Tunability is achieved by adding one or more trimmer capacitors. In our experience, the best Q results when the gap capacitance is uniformly and densely distributed. Unfortunately, the design in Fig. 1C cannot be tuned over a wide range without creating significant capacitance variations along the gap. A further refinement, described as a bridged loop–gap resonator (*49, 50*), has been employed in EPR investigations (Fig. 1D). In this design, the gap capacitor is formed by a continuous conductive strip which bridges across the gap. The resonator is compact, the Q is high, and construction is simple, but resonance typically occurs at a frequency above the NMR range.

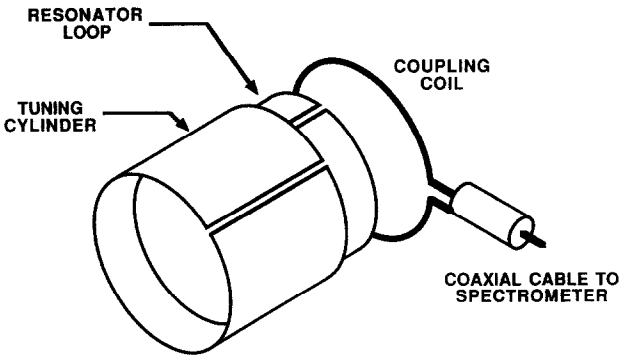

FIG. 2. Partially exploded view of the loop–gap resonator with a concentric tuning cylinder. In use, the ends of the inner resonator and outer tuning cylinder would be coplanar.

IMPROVED LGR DESIGN

We have developed a concentric loop–gap resonator (CLGR) for NMR applications which is related to the bridged LGR in Fig. 1. The gap capacitor is formed by an outer tuning cylinder placed concentrically around the inner "loop" (Fig. 2). Rotation of the outer cylinder dramatically alters the capacitance, producing a very large tuning range. When in use, the ends of the two cylinders are coplanar so the capacitance is distributed uniformly along the gap, yielding maximum Q. The tuning action can be understood by referring to Fig. 3. If the gaps of the inner and outer cylinders are aligned, the capacitance across the inner gap is very small. As the outer cylinder is rotated, a small capacitor C_1 and large capacitor C_2 are formed by the concentric surfaces of the two cylinders. For rotations of only a few degrees, the value of the small capacitor C_1 changes rapidly while that of the large capacitor C_2 remains approximately constant. C_1 and C_2 are connected in series, so the total capacitance $C_T = 1/(C_1^{-1} + C_2^{-1})$. The value of C_T is determined by the separation between the

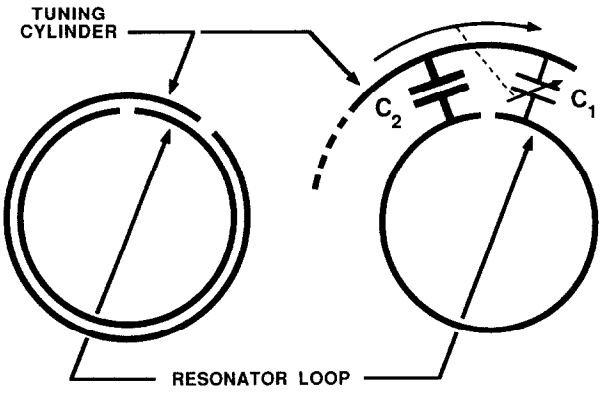

FIG. 3. Schematic representation of the concentric loop–gap resonator tuning mechanism. For small rotations, the large capacitance C_2 is nearly constant.

concentric cylinders, the dielectric employed, and the areas of the conducting surfaces composing C_1 and C_2. The latter depend on the angle of rotation and on the sizes of the inner and outer gaps (Fig. 4A). If the radii of the two cylinders are assumed to be equal, the total capacitance can be represented approximately by

$$C_T = \frac{k}{(\theta - \phi_i)^{-1} + (360° - \theta - \phi_o)^{-1}}, \quad [3]$$

where the rotation angle θ, angle of the inner gap ϕ_i, and angle of the outer gap ϕ_o are defined in Fig. 4A. From Eqs. [1] and [3] the resonance frequency also depends on these angles:

$$\nu = k'\sqrt{(\theta - \phi_i)^{-1} + (360° - \theta - \phi_o)^{-1}}. \quad [4]$$

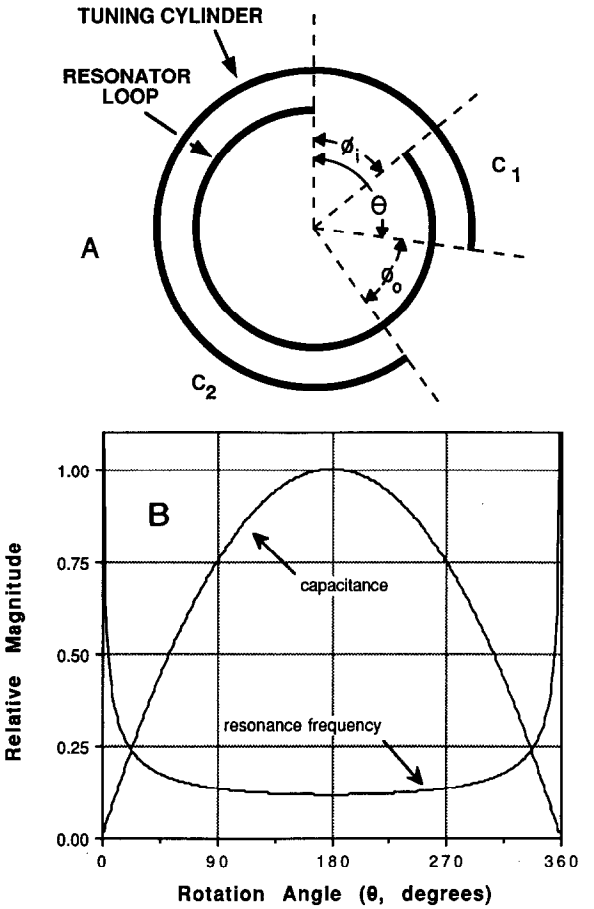

FIG. 4. (A) Definition of angles employed in the series LC model of concentric loop–gap resonator tuning. (B) Theoretical behavior of CLGR capacitance and resonance frequency as a function of tuning cylinder rotation angle θ for infinitely narrow inner and outer gaps ($\phi_i = \phi_o = 0$).

Figure 4B shows the dependence of total capacitance and resonance frequency for a hypothetical CLGR with infinitely narrow gaps ($\phi_i = \phi_o = 0$). The gaps are superimposed at $\theta = 0$. As the outer cylinder is rotated, the capacitance rises rapidly from approximately zero while the resonance frequency drops precipitously. With further rotation, both parameters become less sensitive to changes in θ until the gaps are opposed ($\theta = 180°$), at which point $C_1 = C_2$, C_T is maximum, and ν is minimum. Rotation past this position leads to a symmetrical reversal of the previous behavior. A similar dependence of ν versus θ is found for realistic inner and outer gap sizes. Figure 5 contains plots for $\phi_i = 10°$ and $\phi_o = 10°$, 120°, and 270°. Increasing the outer gap narrows the θ range over which tuning can be varied and changes the angle that gives the minimum resonance frequency. The decrease in C_T resulting from the smaller outer cylinder surface area also produces a somewhat higher minimum resonance frequency. Overall, the tuning characteristics are rather tolerant of variations in construction, and precise fabrication techniques are not required to produce a functional resonator.

As shown in Figs. 4 and 5, much of the tuning range of the CLGR occurs over a narrow band of rotation angles where either C_1 or C_2 is small. This provides an enormous potential tuning range. However, tuning to a precise, arbitrary frequency can be difficult unless the target value lies within the broad minimum of the tuning curve. We have therefore employed an additional concentric tuning cylinder which is useful for fine tuning (Fig. 6). This outer, fine-tuning cylinder can be separated from the other parts of the resonator by a thick dielectric layer. Coarse tuning to a frequency slightly above the target value is first accomplished using the middle cylinder, which is then immobilized. The outer (and easily accessible) cylinder is available for tuning over a smaller range to achieve exact resonance and to compensate for frequency

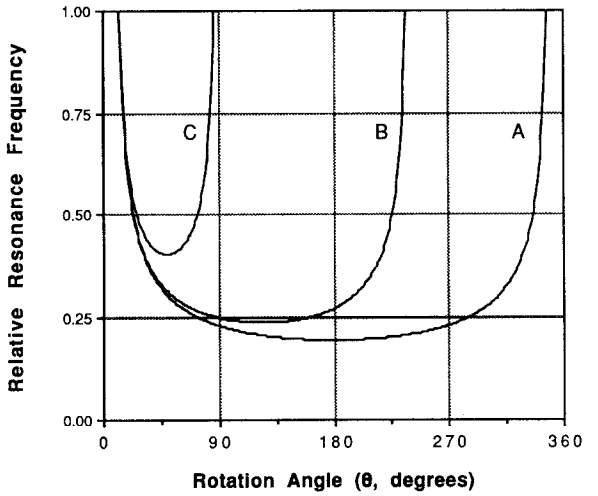

FIG. 5. Dependence of CLGR resonance frequency on rotation angle θ and outer gap size of the tuning cylinder. The inner gap $\phi_i = 10°$ for all plots. (A) $\phi_o = 10°$. (B) $\phi_o = 120°$. (C) $\phi_o = 270°$.

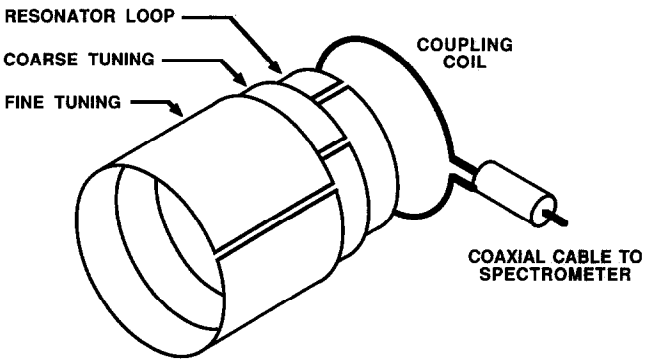

FIG. 6. Partially exploded view of the complete concentric loop–gap resonator, including a coarse-tuning cylinder and an outer, fine-tuning cylinder. Adjusting the angle of the coarse cylinder produces resonance just above the target frequency, and final adjustments are performed using the outer cylinder.

changes due to differences in loading, etc. With reasonable choices for resonator dimensions and dielectric thickness, the tuning can be controlled with good precision over an approximately fourfold range. If necessary, this range can be extended further by using an additional fine-tuning cylinder.

EXPERIMENTAL

A concentric loop–gap resonator of the above design was constructed in our laboratory for use in ^{1}H and ^{19}F imaging and spectroscopy experiments at 4.7 T. The diameter of the resonator loop was 61 mm and the length was 52 mm. The inner gap was 3.0 mm (5.6°) across. To fabricate the loop, a self-adhesive 2 oz. copper sheet (Bishop Graphics, Canoga Park, California) was mounted on cylindrical high-density polyethylene dielectric having a thickness of approximately 0.7 mm. This dielectric material was obtained by cutting the ends off a Nalgene No. 2104, 250 ml, narrow-mouth bottle. Polyethylene is a suitable dielectric material for this application due to its low loss tangent and adequate electric strength (*53*), which enable it to be used in high-Q resonance circuits at high-RF power levels. Two outer tuning cylinders were constructed from the same materials as the inner loop and were split longitudinally to allow them to fit over it. The coarse-tuning cylinder (Fig. 6) had a 63 mm diameter, 52 mm length, and 7.5 mm (13.6°) gap. The outer, fine-tuning cylinder was 68 mm in diameter, 52 mm in length, and had a 74 mm (125°) gap. An extra layer of polyethylene was inserted between the two cylinders to reduce the tuning sensitivity during rotation of the outermost collar. Rubber bands were used to hold each of the two movable cylinders in place, with no appreciable reduction in Q attributable to the rubber. An untuned, two-turn coupling loop of 61 mm diameter was mounted as shown in Fig. 6. Matching to 50 ohms was accomplished by adjusting the distance between the coupling loop and the end of the resonator within a range of 0.2 to 3 cm. [Reference (*46*) describes an elegant mechanism for this purpose.] The entire resonator assembly was mounted in an acrylic plastic holder for convenient positioning inside the magnet bore.

The RF field homogeneity inside the concentric loop–gap resonator was determined. The resonator was driven at 188 MHz with a signal generator, and an oscilloscope was used to measure the voltage induced in an untuned "search" coil (6 mm diameter) oriented with its longitudinal axis parallel to that of the CLGR. As shown in Fig. 7, the homogeneity was excellent. Radial RF homogeneity was ±10% within the central 80% of the diameter (Fig. 7B). When measured along the longitudinal axis (Fig. 7A), the field was uniform to within ±5% in the central 75% of the resonator volume. Uniformity was ±12% over the entire length, which compares favorably with other coil designs. The maximum RF field was found to be offset from the exact center by several millimeters, probably due to the influence of the coupling loop located approximately two centimeters past the negative extreme of the distance scale in Fig. 7A. This design asymmetry, combined with a finite Q, would produce a slightly greater field in the region nearest the RF source. However, the effect is small in practice.

Figure 8 shows the dependence of resonance frequency on rotation angle for the above resonator. Experimental values agreed well with those predicted from Eq. [4]

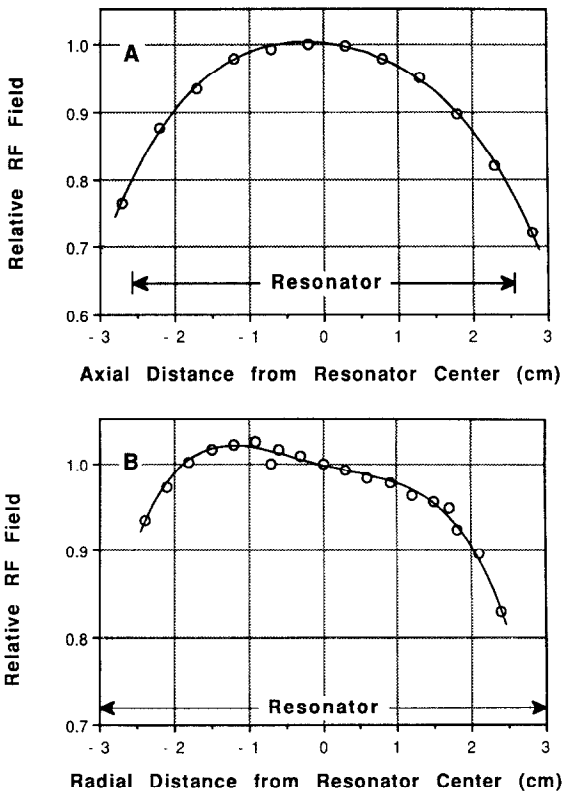

FIG. 7. Experimental RF field plots for the concentric loop–gap resonator. The solid lines, which are intended as guides to the eye, are fourth-order polynomial fits to the data and are without known theoretical justification. (A) Field profile along the longitudinal axis of the resonator. (B) Field profile along an axis passing through the resonator center and orthogonal to the longitudinal axis.

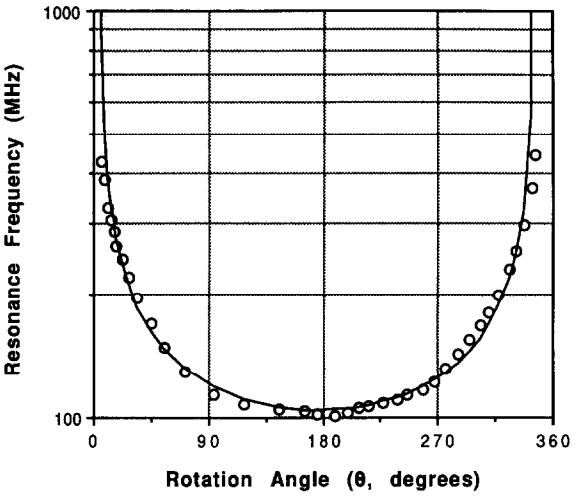

FIG. 8. Unloaded resonance frequency versus coarse-tuning cylinder rotation angle for the experimental concentric loop–gap resonator of Fig. 2. The solid line represents a fit of the data to Eq. [4] using $\phi_i = 5.6°$, $\phi_o = 13.6°$, and $k' = 960.22$. The quality of the fit is good except for points near the extreme ends, where the model fails to predict the capacitance accurately.

except at the extremes, where the inner and outer gaps were nearly coincident. This is undoubtedly due to the simplicity of the theoretical model, which does not include capacitance contributions from parallel surfaces which are in close proximity but not strictly overlapping. The presence of RF fringe fields ensures that some capacitance will be present even if the gaps are perfectly aligned (near $\theta = 0°, 360°$), decreasing the actual resonance frequency relative to the theoretical prediction. In Fig. 8, the experimental resonance frequencies at the most extreme points (7° and 347°) are approximately twofold lower than the theoretical values.

The tuning range and Q of the resonator are influenced by the thickness of dielectric between the tuning cylinder(s) and the inner loop. When a 0.7 mm polyethylene layer was used to separate the inner loop and coarse-tuning cylinder (with no fine-tuning cylinder), the minimum attainable resonance frequency was 101 MHz (Fig. 8). The measured Q was 230 at both 101 and 188 MHz. Increasing the dielectric thickness to 1.7 mm raised the minimum tuning frequency to 138 MHz and increased the Q to 360 for the 138–188 MHz range. A thicker dielectric layer (2.7 mm) produced a higher minimum tuning frequency of 184 MHz but did not improve the Q (360 at 188 MHz).

The number and design of the various tuning cylinders also affect the Q and tuning frequency. When a fine-tuning cylinder with 2.4 mm dielectric layer was added to the inner loop/coarse-tuning cylinder design above, the minimum resonance frequency dropped from 101 to 93 MHz. Rotation of the fine-tuning cylinder enabled precise tuning from 93 to 101 MHz without any coarse adjustment. Q values for this configuration were 210 at 101 MHz and 280 at 188 MHz. Loading the resonator with a 250 g rat reduced the Q to approximately 30 at 188 MHz. A further reduction in resonance

frequency was achieved for the same inner loop dimensions by using a coarse-tuning cylinder with two overlapping layers (Fig. 9). Since one of these layers bridges the gap of the inner loop for all rotation angles, the upper frequency limit is greatly reduced. In this particular case, the tuning range was 53 to 60 MHz (Q = 200) without the fine-tuning cylinder. When the latter was added, the complete tuning range became 50 to 60 MHz (Q = 190) for all combinations of coarse and fine cylinder angles. Loading the resonator with a 125 ml bottle of 0.9% NaCl (aq) reduced the Q to 40. For the design in Fig. 9, the number of layers determines the center of the tuning frequency range. The spiral geometry permits the copper surface to be terminated at any arbitrary angle so the number of layers can be nonintegral. It is therefore possible to construct a resonator with the desired tuning frequency for a wide range of inner loop dimensions.

NMR performance characteristics for the concentric loop–gap resonator design in Fig. 6 were measured using a Bruker Biospec 47/30 imaging/spectroscopy system (Bruker Instruments, Billerica, Massachusetts) equipped with an AMT Model M3205 RF power amplifier (American Microwave Technology, Inc., Fullerton, California). The measured RF pulse power at the ^{19}F resonance frequency (188.4 MHz) was 120 W. Three aqueous 154 mM sodium fluoride samples with different volumes were employed. All samples were cylindrical and had the same length (40 mm), but the diameter was varied to change the resonator loading and to examine the effects of B_1 inhomogeneity. Table 1 shows experimental values for several ^{19}F NMR parameters measured as a function of sample diameter. The 90° RF pulse width increased with loading and correlated with a reduction in Q. To assess the resonator's RF homogeneity,

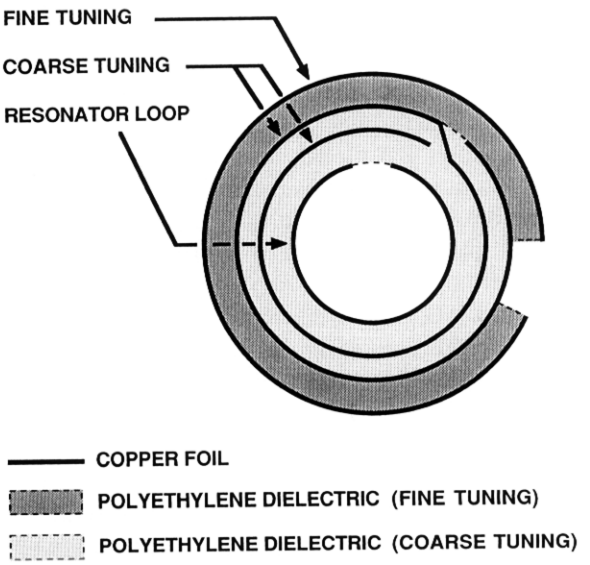

FIG. 9. Cross-sectional view (not to scale) of a concentric loop–gap resonator incorporating a two-layer coarse-tuning cylinder to lower the resonance frequency. Several layers of copper may be used, and the foil may be terminated at any angle to yield a nonintegral number of layers.

TABLE 1

Performance Characteristics of the Concentric Loop–Gap Resonator[a]

Sample diameter (mm)	Sample volume (ml)[b]	Q[c]	90° pulse width (μs)	$A_{90°}/A_{180°}$[d]	Relative area/noise[e]	Relative volume × $Q^{1/2}$[f]
13	5.3	238	22	29.9	0.23	0.23
31	28.1	101	42	9.4	0.85	0.79
48	70.4	25.7	88	2.8	1.00	1.00

[a] Using the 52 mm (length) × 61 mm (i.d.) resonator of Fig. 6 with 0.7 mm dielectric between the inner loop and coarse-tuning cylinder. The coarse- and fine-tuning cylinders were separated by a 1.7 mm dielectric layer. RF power was 120 W at 188.4 MHz.

[b] Calculated from the weight of 154 m*M* NaF (aq) contained inside the resonator.

[c] Unloaded Q = 280. Measured using a Wavetek Model 1062 RF sweeper and Wiltron Model 62BF50 VSWR bridge.

[d] Ratio of the ^{19}F NMR signal amplitudes obtained from 90° and 180° pulses.

[e] Calculated from ^{19}F NMR signal areas and peak-to-peak noise amplitudes for each sample. Estimated uncertainty, ±20%.

[f] Relative sample volume × $Q^{1/2}$, calculated from values in columns 2 and 3.

the quality of the "null" NMR signal produced by a 180° pulse was investigated. This signal typically contained both positive and negative components. Therefore, the difference between the maximum positive and negative excursions from zero was taken as its amplitude. The signal amplitude produced by a 90° pulse was divided by the amplitude of the null signal to yield the ratio $A_{90°}/A_{180°}$ tabulated in Table 1. This ratio gives a practical measure of the RF field homogeneity over the sample. As may be seen from the table, homogeneity for the smallest sample was excellent, producing a null signal which was only about 3% of the amplitude obtained using a 90° pulse. However, the homogeneity deteriorated as the sample diameter approached that of the resonator. Figure 7B shows that the RF field decreases rapidly near the resonator wall, yielding a range of nutation angles over large samples for any pulse width. The quality of the null therefore suffers for samples of large diameter. Table 1 also shows the effect of increasing sample volume on the ^{19}F NMR sensitivity. For a homogeneous RF field, the ratio of NMR signal-to-noise should vary in proportion to the product of the sample volume and $\sqrt{Q}$ (*2*). Within experimental uncertainty, the area-to-noise ratios in Table 1 agree with this prediction for all three sample volumes. Signal areas, instead of amplitudes, were used in these calculations because the areas were less sensitive to differences in static field homogeneity. Variations in the shim were unavoidable since the samples differed in size. For the smallest sample, the full linewidth at half-maximum intensity was 8 Hz, and the ratio of the ^{19}F NMR signal amplitude to the peak-to-peak noise amplitude was 170:1 following a single 90° pulse.

Overall, the concentric loop–gap resonator design has proven to be versatile, robust, and sensitive in NMR experiments. It is very easy to construct, and its resonance properties are quite tolerant of errors during fabrication. The chief disadvantage is the longitudinal B_1 field geometry, which requires that the resonator be mounted trans-

versely inside the superconducting magnet bore. However, in many applications the inconvenience is slight, especially in view of the other attributes of the design. In our laboratory, this is presently the coil of choice for ^{19}F imaging in small animals at 188 MHz and for NMR experiments which require excellent RF field homogeneity.

ACKNOWLEDGMENTS

The authors thank Mr. Colin Cook of the Harvard Joint Center for Magnetic Resonance for constructing the plastic holder used to position the resonator inside the magnet bore. This work was supported by a grant from the Whitaker Foundation (Mechanicsburg, Pennsylvania).

REFERENCES

1. H.-J. SCHNEIDER AND P. DULLENKOPF, *Rev. Sci. Instrum.* **48,** 68 (1977).
2. D. I. HOULT AND R. E. RICHARDS, *J. Magn. Reson.* **24,** 71 (1976).
3. C. G. FRY, J. H. IWAMIYA, T. M. APPLE, AND B. C. GERSTEIN, *J. Magn. Reson.* **63,** 214 (1985).
4. D. M. GINSBERG AND M. J. MELCHNER, *Rev. Sci. Instrum.* **41,** 122 (1970).
5. D. I. HOULT AND R. E. RICHARDS, *Proc. R. Soc. London A* **344,** 311 (1975).
6. J. P. BOEHMER, R. I. PRINCE, AND R. W. BRIGGS, *J. Magn. Reson.* **83,** 152 (1989).
7. C. E. HAYES, W. A. EDELSTEIN, J. F. SCHENCK, O. M. MUELLER, AND M. EASH, *J. Magn. Reson.* **63,** 622 (1985).
8. P. M. JOSEPH AND J. E. FISHMAN, *Med. Phys.* **12,** 679 (1985).
9. P. M. JOSEPH AND D. LU, *IEEE Trans. Med. Imaging* **8,** 286 (1989).
10. P. M. JOSEPH AND R. M. SUMMERS, *J. Magn. Reson.* **68,** 198 (1986).
11. J. TROPP, *J. Magn. Reson.* **82,** 51 (1989).
12. D. BALLON, M. C. GRAHAM, S. MIODOWNIK, AND J. A. KOUTCHER, *J. Magn. Reson.* **90,** 131 (1990).
13. L. BOLINGER, M. G. PRAMMER, AND J. S. LEIGH, *J. Magn. Reson.* **81,** 162 (1988).
14. A. R. RATH, *J. Magn. Reson.* **86,** 488 (1990).
15. K. DERBY, J. TROPP, AND C. HAWRYSZKO, *J. Magn. Reson.* **86,** 645 (1990).
16. G. ISAAC, M. D. SCHNALL, R. E. LENKINSKI, AND K. VOGELE, *J. Magn. Reson.* **89,** 41 (1990).
17. J. J. H. ACKERMAN, T. H. GROVE, G. G. WONG, D. G. GADIAN, AND G. K. RADDA, *Nature* **283,** 167 (1980).
18. J. ROUSSEAU, P. LECOUFFE, AND X. MARCHANDISE, *Magn. Reson. Imaging* **8,** 517 (1990).
19. J. L. EVELHOCH, M. G. CROWLEY, AND J. J. H. ACKERMAN, *J. Magn. Reson.* **56,** 110 (1984).
20. A. HAASE, W. HANICKE, AND J. FRAHM, *J. Magn. Reson.* **56,** 401 (1984).
21. M. R. BENDALL AND R. E. GORDON, *J. Magn. Reson.* **53,** 365 (1983).
22. A. J. SHAKA AND R. FREEMAN, *J. Magn. Reson.* **59,** 169 (1984).
23. R. TYCKO AND A. PINES, *J. Magn. Reson.* **60,** 156 (1984).
24. J. PEKAR, J. S. LEIGH, JR., AND B. CHANCE, *J. Magn. Reson.* **64,** 115 (1985).
25. K. R. METZ AND R. W. BRIGGS, *J. Magn. Reson.* **64,** 172 (1985).
26. M. GARWOOD, T. SCHLEICH, B. D. ROSS, G. B. MATSON, AND W. D. WINTERS, *J. Magn. Reson.* **65,** 239 (1985).
27. D. I. HOULT, *J. Magn. Reson.* **33,** 183 (1979).
28. M. GARWOOD, T. SCHLEICH, G. B. MATSON, AND G. ACOSTA, *J. Magn. Reson.* **60,** 268 (1984).
29. J. P. BOEHMER, K. R. METZ, AND R. W. BRIGGS, *J. Magn. Reson.* **62,** 322 (1985).
30. K. R. METZ AND J. P. BOEHMER, *Magn. Reson. Imaging* **6**(1), 53 (1988).
31. J. P. BOEHMER, K. R. METZ, J. MAO, AND R. W. BRIGGS, *Magn. Reson. Med.* **16,** 335 (1990).
32. J. L. ALLIS, P. STYLES, T. A. D. CADOUX-HUDSON, AND B. RAJAGOPALAN, *J. Magn. Reson.* **92,** 158 (1991).
33. W. W. MACALPINE AND R. O. SCHILDKNECHT, *Proc. IRE* **47,** 2099 (1959).
34. S. KAN, P. GONORD, C. DURET, J. SALSET, AND C. VIBET, *Rev. Sci. Instrum.* **44,** 1725 (1973).
35. H.-J. SCHNEIDER AND P. DULLENKOPF, *Rev. Sci. Instrum.* **48,** 832 (1977).
36. J. J. VAN VAALS AND A. H. BERGMAN, *J. Magn. Reson.* **89,** 331 (1990).
37. D. W. ALDERMAN AND D. M. GRANT, *J. Magn. Reson.* **36,** 447 (1979).

38. T. A. CROSS, S. MULLER, AND W. P. AUE, *J. Magn. Reson.* **62,** 87 (1985).
39. A. LEROY-WILLIG, L. DARRASSE, J. TAQUIN, AND M. SAUZADE, *Magn. Reson. Med.* **2,** 20 (1985).
40. V. J. SANK, C.-N. CHEN, AND D. I. HOULT, *J. Magn. Reson.* **69,** 236 (1986).
41. K. YODA AND M. KUROKAWA, *J. Magn. Reson.* **81,** 284 (1989).
42. E.-J. NIJHOF, *Magn. Reson. Imaging* **8,** 345 (1990).
43. W. N. HARDY AND L. A. WHITEHEAD, *Rev. Sci. Instrum.* **52,** 213 (1981).
44. T. M. GRIST AND J. S. HYDE, *J. Magn. Reson.* **61,** 571 (1985).
45. J. P. HORNAK AND J. H. FREED, *J. Magn. Reson.* **62,** 311 (1985).
46. L. D. HALL, T. MARCUS, C. NEALE, B. POWELL, J. SALLOS, AND S. L. TALAGALA, *J. Magn. Reson.* **62,** 525 (1985).
47. J. P. HORNAK, T. L. CECKLER, AND R. G. BRYANT, *J. Magn. Reson.* **68,** 319 (1986).
48. A. JESMANOWICZ, W. FRONCISZ, T. W. GRIST, AND J. S. HYDE, *Magn. Reson. Med.* **3,** 76 (1986).
49. S. PFENNINGER, J. FORRER, A. SCHWEIGER, AND T. WEILAND, *Rev. Sci. Instrum.* **59,** 752 (1988).
50. S. PFENNINGER, J. FORRER, A. SCHWEIGER, AND T. WEILAND, *Phys. Med.* **2–4,** 203 (1989).
51. S. RAMO, J. R. WHINNERY, AND T. VAN DUZER, "Fields and Waves in Communications Electronics," p. 192, Wiley, New York, 1984.
52. S. RAMO, J. R. WHINNERY, AND T. VAN DUZER, "Fields and Waves in Communications Electronics," p. 71, Wiley, New York, 1984.
53. D. R. HOLMES, P. BECKLEY, N. G. DOVASTON, E. C. SNELLING, *et al., in* "Electrical Engineer's Reference Book" (M. A. Laughton and M. G. Say, Eds.), 14th ed., p. 5/28, Butterworths, London, 1985.